GUIDED MODES OF HELICAL WAVEGUIDES

JAY GOPALAKRISHNAN AND MICHAEL NEUNTEUFEL

Abstract. This paper studies guided transverse scalar modes propagating through helically coiled waveguides. Modeling the modes as solutions of the Helmholtz equation within the three-dimensional (3D) waveguide geometry, a propagation ansatz transforms the mode-finding problem into a 3D quadratic eigenproblem. Through an untwisting map, the problem is shown to be equivalent to a 3D quadratic eigenproblem on a straightened configuration. Next, exploiting the constant torsion and curvature of the Frenet frame of a circular helix, the 3D eigenproblem is further reduced to a two-dimensional (2D) eigenproblem on the waveguide cross section. All three eigenproblems are numerically treated. As expected, significant computational savings are realized in the 2D model. A few nontrivial numerical techniques are needed to make the computation of modes within the 3D geometry feasible. They are presented along with a procedure to effectively filter out unwanted non-propagating eigenfunctions. Computational results show that the geometric effect of coiling is to shift the localization of guided modes away from the coiling center. The variations in modes as coiling pitch is changed are reported considering the example of a coiled optical fiber.

Key words: helical coiling, bent waveguide, optical fiber, eigenvalue, dimension reduction, torsion
MSC2020: 78M10, 65F15.

1. Introduction

Waveguides are often bent, deformed, or coiled for varied purposes, such as to fit it into a desired space, for tuning its resonances to desired frequencies, or obtaining better separation of fundamental mode from higher-order modes. Examples include acoustic wave propagation of sound waves in moulded pipes of a musical instrument, and light wave propagation in coiled optical fibers or gas-filled laser fiber amplifiers. This paper develops a theoretical model for computing the guided modes of a helically coiled waveguide, taking into account its specific geometry. Although leaky modes and confinement loss of deformed waveguides are also of great interest, the scope of this work is limited to perfectly guided modes of no loss and considers only waveguides which admit such a boundary condition.

A straight (unbent) waveguide is translationally invariant in its longitudinal propagation direction. Then the three-dimensional (3D) domain it occupies admits separation of variables, which allows one to obtain natural solutions, called (propagating) modes, that propagate along the longitudinal direction, maintaining the same transverse profile on waveguide cross sections. Moreover, the invariant transverse profile can be found by solving a dimension-reduced equation on the two-dimensional (2D) transverse cross section. The dimension reduction (from 3D to 2D) is very attractive for practical computations. The main question we seek to answer in this paper is whether such 2D modes (exist and) are also computable for helical waveguides. The approach we follow is to find an "unbending map" that transforms the helical waveguide into a straight one, and then apply the known techniques on the straightened configuration.

To the best of our knowledge, this is the first work to clarify the role of torsion, in addition to curvature, while computing propagating helical transverse modes. Arguing that such modes, due to the torsion of the helix, must incorporate a cross-sectional rotation while propagating, we develop an ansatz for the modes. This then leads us to the dimension reduction to a 2D eigenproblem for the modes. Informally, using the divergence (div) and gradient (grad) operators on the waveguide cross section, the 2D eigenproblem for a mode ψ with propagation constant β takes the form $\mathrm{div}(J\mathcal{A}\,\mathrm{grad}\,\psi) + Jk^2n^2\psi + \hat{\imath}\beta\mathrm{div}(Jr\psi) + \hat{\imath}\beta Jr\cdot\mathrm{grad}\,\psi = \beta^2 J^{-1}\psi$ where n is the waveguide material coefficient, k is the operating wavenumber, and $J, \mathcal{A}$ and r are extra coefficients which depend on torsion and curvature of the geometry of helical deformation. (See the more precise statements later in (4.7) and Theorem 4.2.) Circularly bent waveguides (with no torsion) have been extensively investigated in the optical literature [6, 8, 9, 17]. All these works model the bent waveguide as a ring, or a torus, with the terminal and initial cross sections fused. In practice, however, long waveguides are coiled at some pitch. Our model can take into account the effects of both the bend radius and the pitch. Moreover, prior works used simplified terms potentially justifiable under a slow bend assumption, an assumption that we have no need for. We will show a relationship between our model and the prior state-of-the-art as the geometry approaches a limiting case of no torsion.

How transverse mode profiles change under circular bending is a well-studied topic in optics since optical fibers are often coiled in spools. It is interesting to note that in solid-state waveguides, like dielectric optical fibers, elastic stresses caused by bending can change the fiber's refractive index. As a fiber bends around some center (like the center of the spool), according to the laws of photoelasticity [12], the fiber's refractive index is expected to increase toward the center (where the material is compressed) and decrease away from the center (where the material is pulled in tension). Hence, one expects the localization of the fundamental mode profile to shift toward the center of the bend where the index is higher, if only the stress-optic effects are taken into consideration. However, there is also a purely mathematical or geometric effect on the mode due to the bend. The fundamental mode profile *shifts exactly in the opposite way,* localizing away from the center of the bend, if only geometric effects are taken into account, as will be abundantly clear from our results in §5. This work is devoted only to capturing the geometric effect accurately. The mode shift seen in reality will depend on which among the photoelastic shift and the geometric shift dominates. The strength of the photoelastic effect depends on the Pockel coefficients of the underlying materials. It takes no effort to modify the refractive index to account for photoelasticity in our model (once the material making up the waveguide is known) since our theory admits such variations in index profiles.

In this study, we have limited our scope to guided modes. The main resulting drawback is that bend losses (which inevitably exist in dielectric fibers [10]) cannot be extracted from computed eigenvalues from the formulation proposed here. This drawback may be rectifiable to some extent by using the beam propagation method into which the mode profiles computed here can be fed in, and losses backed out. Nonetheless, a more mathematically elegant approach would be through an eigenvalue formulation that produces a confinement loss factor from the imaginary part of a computed eigenvalue. To accomplish this, new formulations with absorbing boundary conditions suitable for helical waveguides may be needed. This is an interesting topic for further study, not addressed in this paper.

It is natural to ask if more general waveguide deformations beyond helical ones can be treated using the techniques presented here. This is not clear to us. In the proof of our main theorem (Theorem 4.2) accomplishing the dimension reduction, we make essential use of the fact that the torsion and curvature of a helix are constant. By the fundamental theorem of space curves [3] in differential geometry, circular helices are the only curves in $\mathbb{R}^3$ with constant torsion and curvature. This gives us pause in attempting to generalize the 2D reduction technique to arbitrarily deformed waveguides.

In the next section (§2), we start by modeling the helically bent waveguide as a tubular expansion of an infinite helix curve. Seeking solutions of the Helmholtz equation within such a domain under zero sources, we derive, after some geometric preliminaries, a weak form of the resulting boundary value problem and show that it is equivalent to a quadratic eigenproblem. §3 introduces a map that untwists the helical waveguide into a straightened configuration. The eigenproblem on the physical waveguide is then mapped to a 3D quadratic eigenproblem on the straight cylinder. It is then further reduced to a 2D quadratic eigenproblem in §4 after clarifying an ansatz for propagating helical transverse modes. §5 presents discretizations of the 3D and 2D eigenproblems, cross verification of results from the multiple eigenproblems for the modes, discussion of findings, tables of computed propagation constants, plots of computed eigenmodes, and a study of their variations with the pitch of the winding.

2. Guided modes of a helically bent waveguide

We are concerned with helical waveguides of uniformly circular cross section. In this section, we introduce the three-dimensional (3D) geometrical parameters and identify a suitable 3D equation for a propagating mode of the waveguide, taking into account the curvilinear nature of the propagation direction.

2.1. **The geometry.** We model the waveguide geometry by thickening an infinite helix curve. Accordingly, first let $\gamma : \mathbb{R} \to \mathbb{R}^3$ be a circular helix curve, parameterized by

$$\gamma(s) = \begin{bmatrix} a_{\mathrm{H}} \cos(s/l) \\ a_{\mathrm{H}} \sin(s/l) \\ b_{\mathrm{H}} s/l \end{bmatrix}, \qquad l = \sqrt{a_{\mathrm{H}}^2 + b_{\mathrm{H}}^2}, \tag{2.1}$$

(see Figure 1) for some $a_{\mathrm{H}}, b_{\mathrm{H}} > 0$. It is easily verified that $\gamma(s)$ is an arclength parameterization. Note that its trace $\mathcal{S}$, the image of γ, has no self-intersections, and that γ is a one-to-one onto map. The radius a_{H} is called the "bend radius" or "coiling radius." The "pitch" of the helix γ (or the height of one turn of the helix) is $2\pi b_{\mathrm{H}}$ and its "slope" is $b_{\mathrm{H}}/a_{\mathrm{H}}$, made by the angle

$$\alpha = \tan^{-1}\left(\frac{b_{\mathrm{H}}}{a_{\mathrm{H}}}\right), \tag{2.2}$$

also marked in Figure 1. It is evident from the figure that the length of one turn of the helix equals $L = 2\pi l$. Moreover, $\gamma(s)$ is periodic with L being the period.

Next, consider the Frenet frame of γ. The tangent vector $T(s) = d\gamma/ds$ has unit length since we parameterized the curve by arclength. Henceforth we abbreviate d/ds by "$\prime$", a prime. Since $T'(s) \neq 0$, the "Frenet normal" is the normalized vector

$$N(s) = \frac{T'(s)}{\|T'(s)\|}. \tag{2.3}$$

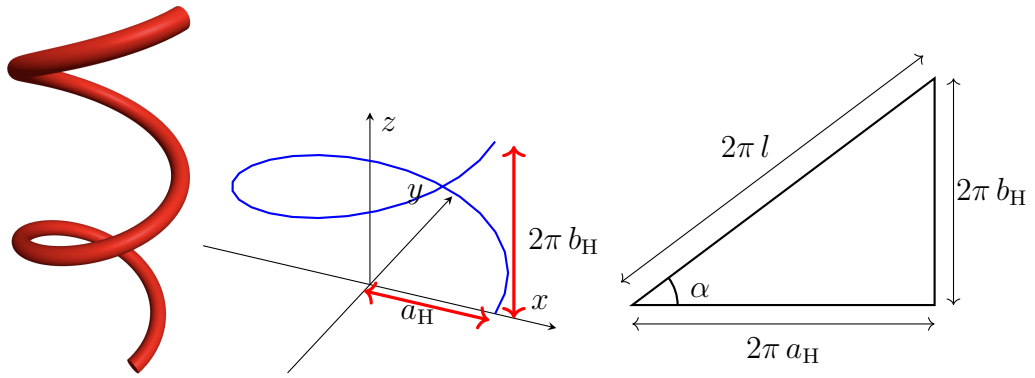

FIGURE 1. *Left:* A helical waveguide. *Middle:* The set $\mathcal{S}$ giving the geometry of the waveguide centerline, i.e., the image of γ. *Right:* If the cylinder containing the curve $\mathcal{S}$ is unwrapped, the right triangle shown is obtained.

Throughout, we use $X \cdot Y$ and $\|X\|$, respectively, to refer to the Euclidean inner product and norm for any $X, Y \in \mathbb{R}^3$. The moving Frenet frame is then the triple of vector fields $(T(s), N(s), B(s))$, where $B = T \times N$ denotes the binormal vector. Also, recall that the Frenet structure equations read

$$T' = \kappa_n\, N - \kappa_g\, B, \qquad N' = -\kappa_n\, T + \tau\, B, \qquad B' = \kappa_g\, T - \tau\, N, \tag{2.4}$$

where κ_g, κ_n, and τ are the geodesic curvature, the normal curvature, and the torsion, respectively. In particular, since T' is in the direction of N by (2.3) and $T \cdot B = T \cdot N = 0$, the last equation of (2.4) implies

$$\kappa_g = B' \cdot T = -T' \cdot B = 0, \tag{2.5a}$$

while the first equation of (2.5) shows that

$$\kappa_n = T' \cdot N = -N' \cdot T = \|T'(s)\|. \tag{2.5b}$$

The remaining equation of (2.4) gives

$$\tau = N' \cdot B = -B' \cdot N. \tag{2.5c}$$

The (total) curvature κ of a curve is the quantity

$$\kappa = \sqrt{\kappa_g^2 + \kappa_n^2}. \tag{2.6}$$

The Frenet frame and all quantities in the structure equations can be immediately computed using the parameterization $\gamma(s)$ and the above formulas. Namely,

$$T = \frac{1}{l}\begin{bmatrix} -a_{\mathrm{H}} \sin(s/l) \\ a_{\mathrm{H}} \cos(s/l) \\ b_{\mathrm{H}} \end{bmatrix}, \qquad N = -\begin{bmatrix} \cos(s/l) \\ \sin(s/l) \\ 0 \end{bmatrix}, \qquad B = \frac{1}{l}\begin{bmatrix} b_{\mathrm{H}} \sin(s/l) \\ -b_{\mathrm{H}} \cos(s/l) \\ a_{\mathrm{H}} \end{bmatrix}. \tag{2.7}$$

Using trigonometric identities involving the slope angle in (2.2),

$$\sin(\alpha) = \frac{b_{\mathrm{H}}}{l}, \qquad \cos(\alpha) = \frac{a_{\mathrm{H}}}{l} \tag{2.8}$$

we may also rewrite the above expressions in terms of the slope angle. The resulting torsion and geodesic curvature, normal curvature, and total curvature equal

$$\tau = \frac{\sin(\alpha)}{l}, \qquad \kappa_g = 0, \qquad \kappa_n = \kappa = \frac{\cos(\alpha)}{l} = \frac{a_{\mathrm{H}}}{a_{\mathrm{H}}^2 + b_{\mathrm{H}}^2}. \tag{2.9}$$

by (2.5) and (2.6).

Next, we thicken the curve to obtain a waveguide. Let $D(s)$ denote the open disk of radius R, centered at $\gamma(s)$, and lying in the plane passing through $\gamma(s)$ with its normal vector equal to $T(s)$. We refer to R as the "waveguide radius", which is distinct from the "bend radius" a_{H}. *We assume that R is small enough so that these transverse disks are all disjoint,* i.e.,

$$D(s_1) \cap D(s_2) = \varnothing, \quad \text{for all } s_1 \neq s_2. \tag{2.10}$$

All our results are under this assumption, which is henceforth tacitly understood to hold. The infinite helical waveguide occupies the domain formed by the disjoint union of these transverse disks,

$$\Omega = \bigsqcup_{s\in\mathbb{R}} D(s).$$

Locally, near any point of the curve, the assumption (2.10) constrains R inversely in terms of the curvature of γ. Specifically,

$$R < \frac{a_{\mathrm{H}}^2 + b_{\mathrm{H}}^2}{a_{\mathrm{H}}} = \frac{1}{\kappa} \tag{2.11}$$

is one of the two sufficient conditions stated in [15] (see also [13]) to ensure that a helical waveguide is not self-intersecting, as required by (2.10). For an alternate justification of the assumption (2.11), see Remark 3.2 later. Assumption (2.10) is also a global constraint. A uniform finite bound on the curvature alone is not sufficient to determine an R for which (2.10) holds.

In view of the assumption (2.10), any point $(x, y, z) \in \Omega$ belongs to exactly one disk $D(s)$ whose center is $\gamma(s)$. Hence, the mapping that takes any $(x, y, z) \in \Omega$ to its unique centerline point $\gamma(s)$ is well defined, namely

$$P:\ \Omega \to \gamma, \qquad P(x, y, z) = \gamma(s) \quad \text{for any } (x, y, z) \in D(s). \tag{2.12}$$

It gives the closest point projection onto the curve γ. We also need a mapping from (x, y, z) to its centerline arclength value s, namely

$$S:\ \Omega \to \mathbb{R}, \qquad S(x, y, z) = s \quad \text{for any } (x, y, z) \in D(s), \tag{2.13a}$$

which is again a proper definition since each $(x, y, z) \in \Omega$ belongs to exactly one $D(s)$. Since $\gamma : \mathbb{R} \to \mathcal{S} \equiv \gamma(\mathbb{R})$ is a one-to-one and onto map (extendable smoothly to a tubular neighborhood of the curve), the inverse map $\gamma^{-1} : \mathcal{S} \to \mathbb{R}$ exists and is smooth. Applying γ^{-1} to both sides of the equation in (2.12), we find that

$$S = \gamma^{-1} \circ P, \tag{2.13b}$$

an alternative representation of S. We do not have a closed form expression for S or P. Except when the helix degenerates to a straight or toroidal waveguide, one cannot expect analytical expressions for them since a transcendental equation must be solved. In §5.2 we present a procedure to approximate S numerically. We proceed to use S to develop a mode ansatz in the next subsection.

2.2. **Modes as eigenfunctions.** We are interested in modes propagating along the helical waveguide Ω. They are modeled as solutions of the Helmholtz equation within the waveguide with zero sources. Specifically, given a material coefficient function $n : \Omega \to \mathbb{R}$ and a wavenumber $k > 0$, we are interested in finding a function $u : \Omega \to \mathbb{C}$ satisfying

$$\Delta u + k^2 n^2 u = 0, \quad \text{in } \Omega, \tag{2.14a}$$

$$u = 0, \quad \text{on } \partial\Omega. \tag{2.14b}$$

Such waveguide modes arise when studying time-harmonic wave propagation within Ω. We may think of u as modeling a pressure variable in acoustic wave propagation of sound waves in tubes, or a polarization-maintaining electromagnetic wave in coiled optical fibers. Our notation in (2.14a) is closer to the optical fiber application where n can be interpreted as the optical refractive index.

Of particular interest are modes that propagate in a curvilinear direction through the waveguide. They have the form

$$u(x, y, z) = e^{\hat{\imath}\beta\varphi(x,y,z)} U(x, y, z) \tag{2.15}$$

for some propagation constant β and some smooth phase function φ that determines the wavefronts. Here $\hat{\imath}$ denotes the imaginary unit. Given a u, there are obviously multiple ways to rewrite it in terms of a U and a φ as in (2.15). A specific φ of interest will be specified shortly, but we begin with an elementary observation that holds for any smooth φ.

Proposition 2.1. *If u in the form (2.15) solves (2.14), then $U = 0$ on $\partial\Omega$ and*

$$\Delta U + \hat{\imath}\beta \mathrm{div}(U\nabla\varphi) + \hat{\imath}\beta\nabla\varphi \cdot \nabla U + (k^2 n^2 - \beta^2 \|\nabla\varphi\|^2) U = 0, \quad \text{in } \Omega. \tag{2.16}$$

Proof. By the product rule,

$$\nabla u = e^{\hat{\imath}\beta\varphi} \left(\nabla U + \hat{\imath}\beta U \nabla\varphi\right),$$
$$\Delta u = e^{\hat{\imath}\beta\varphi} \left(\Delta U + \hat{\imath}\beta \mathrm{div}(U\nabla\varphi) + (\hat{\imath}\beta\nabla U - \beta^2 U\nabla\varphi) \cdot \nabla\varphi\right),$$

so (2.16) follows by substituting these into (2.14a). □

Next, we refine the ansatz (2.15) by selecting a phase φ that is constant on each waveguide cross section. Recall that the S defined in (2.13) is constant on each transverse disk $D(s)$. Hence a solution of (2.14) of the form

$$u(x, y, z) = e^{\hat{\imath}\beta\, S(x,y,z)} U(x, y, z) \tag{2.17}$$

represents a wave that propagates along the fiber, having phases that continuously increase with the arclength s of the waveguide centerline. We are interested in perfectly guided modes (i.e., their energy does not decay as it propagates along the fiber) so we proceed with the understanding that β in (2.17) is a real number. At this point U in the ansatz (2.17) depends on all coordinate variables (but we will refine it further as we proceed). By Proposition 2.1, U in (2.17) solves (2.16) with S in place of φ, i.e.,

$$\Delta U + \hat{\imath}\beta \mathrm{div}(U\nabla S) + \hat{\imath}\beta\nabla S \cdot \nabla U + (k^2 n^2 - \beta^2 \|\nabla S\|^2) U = 0 \qquad \text{in } \Omega, \tag{2.18a}$$

$$U|_{\partial\Omega} = 0 \tag{2.18b}$$

for a sufficiently regular function U.

The system (2.18) is a quadratic eigenvalue problem for β and U. We will have more to say about helical transverse propagating modes in §4.1. For now, we conclude this section by writing out a useful weak formulation of (2.18). Let $H^1_{0,\mathrm{loc}}(\Omega)$ denote the standard Sobolev

space of locally square-integrable complex-valued functions on Ω whose first-order derivatives are also locally square-integrable and whose trace vanishes on the boundary $\partial\Omega$. For scalar functions f, g on some measurable domain O, we use $(f,g)_O$ to denote the complex $L^2(O)$ inner product of f and g. Even when f and g are vector fields on O, we continue to use the same notation to denote the integral of their appropriate product, i.e., $(f,g)_O = \int_O f \cdot \overline{g}$. All integrals are computed using the standard Lebesgue measure dx in O, which we omit from the integral notation when no confusion can arise. Let $\mathcal{D}(\Omega)$ denote the space of smooth functions with compact support in Ω. Define, for any $W \in H^1_{0,\mathrm{loc}}(\Omega)$ and $V \in \mathcal{D}(\Omega)$, the following three sesquilinear forms on $H^1_{0,\mathrm{loc}}(\Omega) \times \mathcal{D}(\Omega)$.

$$a(W,V) := (\nabla W, \nabla V)_\Omega - (k^2 n^2 W, V)_\Omega, \tag{2.19a}$$

$$b(W,V) := \hat{\imath}(W\nabla S, \nabla V)_\Omega - \hat{\imath}(\nabla W, V\nabla S)_\Omega, \tag{2.19b}$$

$$c(W,V) := (W\nabla S, V\nabla S)_\Omega. \tag{2.19c}$$

Proposition 2.2 (Eigenproblem on helical waveguide)**.** *In weak form, the boundary value problem* (2.18) *is the problem of finding a quadratic eigenvalue β and its corresponding eigenfunction $U \in H^1_{0,\mathrm{loc}}(\Omega)$ such that*

$$a(U,V) + \beta\, b(U,V) + \beta^2\, c(U,V) = 0, \qquad \textit{for all } V \in \mathcal{D}(\Omega). \tag{2.20}$$

Proof. Multiply (2.18a) by the complex conjugate of a test function $V \in \mathcal{D}(\Omega)$ and integrate over Ω. In the resulting equation, replacing ΔU by $\mathrm{div}(\nabla U)$, there are two terms with the divergence operator. We integrate both by parts. Then, using the compact support of $\mathcal{D}(\Omega)$, the boundary integrals arising from the integration by parts vanish, and we obtain

$$\int_\Omega \nabla U \cdot \nabla \overline{V} + \hat{\imath}\beta \left(U \nabla S \cdot \nabla \overline{V} - \overline{V} \nabla S \cdot \nabla U \right) + \left(\beta^2 \|\nabla S\|^2 - k^2 n^2 \right) U \overline{V} \;=\; 0. \tag{2.21}$$

Rearranging, we obtain (2.20). □

3. An unbending map and a straightened configuration

In this section, we introduce a map Φ that "unbends" the helical deformation of the waveguide. Using it, we show that the previous quadratic eigenproblem (2.20) transforms into a variable coefficient quadratic eigenproblem on a straight cylindrical waveguide, which we shall refer to as the *straightened configuration*.

Recall the normal $N(s)$ and binormal $B(s)$ fields from (2.7). Letting

$$\hat{\Omega} = \{(\hat{x}, \hat{y}, \hat{z}) \in \mathbb{R}^3 \,:\, \hat{x}^2 + \hat{y}^2 < R^2\} \tag{3.1}$$

denote an upright infinite cylinder, define an unbending map that maps the helical waveguide Ω to the straightened configuration $\hat{\Omega}$ by

$$\Phi : \hat{\Omega} \to \Omega, \qquad \Phi(\hat{x}, \hat{y}, \hat{z}) = \gamma(\hat{z}) + \hat{x}\, N(\hat{z}) + \hat{y}\, B(\hat{z}). \tag{3.2}$$

Let $\hat{\Gamma}(s)$ denote the disk obtained by the intersection of the plane $\hat{z} = s$ with $\hat{\Omega}$. Clearly, Φ maps $\hat{\Omega}$ one-to-one onto Ω and furthermore

$$\Phi\big(\hat{\Gamma}(s)\big) = D(s), \qquad s \in \mathbb{R}. \tag{3.3}$$

We use $(\hat{x}, \hat{y}, \hat{z})$ to denote points in $\hat{\Omega}$ and (x, y, z) to denote points in Ω.

Given a function $U(x, y, z)$ on Ω, its pullback by Φ on $\hat{\Omega}$ is the function

$$\hat{U} = U \circ \Phi.$$

Derivative operators are supplied with a hat to indicate differentiation with respect to the variables $\hat{x}, \hat{y}, \hat{z}$ in $\hat{\Omega}$, e.g., $\hat{\nabla}\hat{U} = [\partial_{\hat{x}}\hat{U}, \partial_{\hat{y}}\hat{U}, \partial_{\hat{z}}\hat{U}]^t$. Let $[\hat{\nabla}\Phi]$ denote the Jacobian matrix containing all first-order derivatives of Φ, i.e., $[\hat{\nabla}\Phi] = [\partial_{\hat{x}}\Phi, \partial_{\hat{y}}\Phi, \partial_{\hat{z}}\Phi]$. It is invertible (since Φ is). Let $e_{\hat{z}}$ denote the unit vector in the $\hat{z}$ direction and let

$$\mathcal{C} = [\hat{\nabla}\Phi]^t[\hat{\nabla}\Phi], \quad d = \mathcal{C}^{-1}e_{\hat{z}}, \quad J = \big|\det[\hat{\nabla}\Phi]\big|. \tag{3.4}$$

These quantities will appear in a transformed eigenproblem for $\hat{U}$, so we note the following formulas first.

Lemma 3.1. *For the map Φ in (3.2), the above quantities are given by $J = |1 - \hat{x}\kappa|$,*

$$\mathcal{C} = \begin{bmatrix} 1 & 0 & -\hat{y}\tau \\ 0 & 1 & \hat{x}\tau \\ -\hat{y}\tau & \hat{x}\tau & (1-\hat{x}\kappa)^2 + (\hat{x}^2+\hat{y}^2)\tau^2 \end{bmatrix}, \quad \textit{and} \quad d = J^{-2}\begin{bmatrix} \hat{y}\tau \\ -\hat{x}\tau \\ 1 \end{bmatrix}. \tag{3.5}$$

Proof. Differentiating the vector in (3.2) with respect to $\hat{x}, \hat{y}$, and $\hat{z}$, we obtain the columns of the Jacobian matrix of Φ,

$$\hat{\nabla}\Phi = \begin{bmatrix} N & B & \gamma'(\hat{z}) + \hat{x}N'(\hat{z}) + \hat{y}B'(\hat{z}) \end{bmatrix}.$$

Noting that $\gamma' = T$, the Frenet structure equations of (2.4) imply

$$\hat{\nabla}\Phi = \begin{bmatrix} N & B & (1-\hat{x}\kappa)T + \hat{x}\tau B - \hat{y}\tau N \end{bmatrix}. \tag{3.6}$$

The expression for $\mathcal{C} = [\hat{\nabla}\Phi]^t[\hat{\nabla}\Phi]$ in (3.5) now follows by the orthonormality of T, N, and B. Next, a cofactor expansion of the just obtained expression for $\mathcal{C}$ shows that

$$\det \mathcal{C} = (1-\hat{x}\kappa)^2. \tag{3.7}$$

Since we also know from (3.4) that $\det\mathcal{C} = (\det[\hat{\nabla}\Phi])^2 = J^2$, the stated expression for J follows from (3.7). Finally, to prove the stated expression for d, it suffices to observe that when the matrix and the vector expressions in (3.5) are multiplied and simplified, we find that $\mathcal{C}d = e_{\hat{z}}$. □

Remark 3.2. By Lemma 3.1 and (2.9), the determinant reads

$$J(\hat{x}, \hat{y}, \hat{z}) = |1 - \hat{x}\kappa| = 1 - \frac{\hat{x}}{l}\cos\alpha. \tag{3.8}$$

We have removed the absolute value in the last expression because it is positive: indeed, from (3.1), we know that $\hat{x}^2 + \hat{y}^2 < R^2$, so

$$\hat{x}\kappa < R\kappa < 1$$

due to (2.11). It is interesting to note that what we have just shown, namely

$$J > 0, \tag{3.9}$$

also yields, by the implicit function theorem, the local invertibility of the map Φ. In particular, this gives a justification (different from [15]) of the sufficiency of condition (2.11) to avoid self-intersections for nearby points in the parameter domain $\hat{\Omega}$.

The eigenproblem of Proposition 2.2 on the bent helical waveguide can now be transformed into an eigenproblem on the straight cylinder. The pullback map $U \mapsto \hat{U} = U \circ \Phi$ maps elements in $H^1_{0,\mathrm{loc}}(\Omega)$ one-to-one onto $H^1_{0,\mathrm{loc}}(\hat{\Omega})$. Let

$$\hat{n} = n \circ \Phi, \qquad \hat{a}(\hat{U},\hat{V}) = (J\mathcal{C}^{-1}\hat{\nabla}\hat{U},\hat{\nabla}\hat{V})_{\hat{\Omega}} - (Jk^2\hat{n}^2\hat{U},\hat{V})_{\hat{\Omega}},$$
$$\hat{b}(\hat{U},\hat{V}) = \hat{\imath}(J\hat{U}, d\cdot\hat{\nabla}V)_{\hat{\Omega}} - \hat{\imath}(Jd\cdot\hat{\nabla}\hat{U},\hat{V})_{\hat{\Omega}}, \qquad \hat{c}(\hat{U},\hat{V}) = (J^{-1}\hat{U},\hat{V})_{\hat{\Omega}}.$$

Proposition 3.3 (Eigenproblem on straightened configuration)**.** *An eigenvalue β and corresponding eigenfunction U solves* (2.20) *on the waveguide Ω if and only if β and $\hat{U} = U \circ \Phi \in H^1_{0,\mathrm{loc}}(\hat{\Omega})$ solves*

$$\hat{a}(\hat{U},\hat{V}) + \beta\,\hat{b}(\hat{U},\hat{V}) + \beta^2\,\hat{c}(\hat{U},\hat{V}) = 0, \qquad \text{for all } \hat{V} \in \mathcal{D}(\hat{\Omega}), \tag{3.10}$$

on the straight cylinder $\hat{\Omega}$.

Proof. By the chain rule,

$$\hat{\nabla}\hat{U} = [\hat{\nabla}\Phi]^t(\nabla U)\circ\Phi. \tag{3.11}$$

Using this within a change of variables formula, we obtain

$$\begin{aligned}\int_\Omega \nabla U\cdot\nabla V &= \int_{\hat{\Omega}} [\hat{\nabla}\Phi]^{-t}\hat{\nabla}\hat{U}\cdot[\hat{\nabla}\Phi]^{-t}\hat{\nabla}V\,|\det[\hat{\nabla}\Phi]\,| \\ &= \int_{\hat{\Omega}} ([\hat{\nabla}\Phi]^t[\hat{\nabla}\Phi])^{-1}\hat{\nabla}\hat{U}\cdot\hat{\nabla}\hat{V}\;J.\end{aligned}$$

Replacing V by $\overline{V}$, this shows that $a(U,V) = \hat{a}(\hat{U},\hat{V})$.

Next, consider $b(U,V)$ in (2.19). Since Φ maps $\hat{\Gamma}(s)$ one-to-one onto $D(s)$—see (3.3)—the definition (2.12) of P shows that $(P\circ\Phi)(\hat{x},\hat{y},\hat{z}) = \gamma(\hat{z})$. Hence the definition (2.13) of S shows that

$$(S\circ\Phi)(\hat{x},\hat{y},\hat{z}) = \hat{z}, \tag{3.12}$$

so $\hat{S} = S\circ\Phi$ has $\hat{\nabla}\hat{S} = e_{\hat{z}}$. Hence one of the terms in $b(U,V)$, after applying the change of variables formula, becomes

$$\begin{aligned}(U\nabla S,\nabla V)_\Omega &= (J\hat{U}[\hat{\nabla}\Phi]^{-t}\hat{\nabla}\hat{S},[\hat{\nabla}\Phi]^{-t}\hat{\nabla}\hat{V})_{\hat{\Omega}} \\ &= (J\hat{U}\mathcal{C}^{-1}e_{\hat{z}},\nabla\hat{V})_{\hat{\Omega}} = (J\hat{U},d\cdot\nabla\hat{V})_{\hat{\Omega}}.\end{aligned}$$

Handling the other term of $b(U,V)$ similarly, we show that $b(U,V) = \hat{b}(\hat{U},\hat{V})$.

Finally, for the third sesquilinear form $c(U,V)$,

$$\begin{aligned}c(U,V) = (U\nabla S, V\nabla S)_\Omega &= (J\hat{U}[\hat{\nabla}\Phi]^{-t}\hat{\nabla}\hat{S},\hat{V}[\hat{\nabla}\Phi]^{-t}\hat{\nabla}\hat{S})_{\hat{\Omega}} \\ &= (J(e_{\hat{z}}\cdot\mathcal{C}^{-1}e_{\hat{z}})\hat{U},\hat{V})_{\hat{\Omega}}.\end{aligned}$$

By Lemma 3.1, $e_{\hat{z}}\cdot\mathcal{C}^{-1}e_{\hat{z}} = e_{\hat{z}}\cdot d = J^{-2}$ showing that $c(U,V) = \hat{c}(\hat{u},\hat{v})$. □

4. Dimension reduction

In this section, we introduce a 2D eigenproblem for transverse modes under further assumptions and show how it can be derived from the prior 3D eigenproblem.

A basic question we must grapple with is what constitutes a transverse mode in a helical waveguide. The difficulty is that the torsion of the helix creates a natural rotation of the cross section as one proceeds in the propagating direction. Therefore, unlike straight waveguides

where transverse modes do not vary in the propagating direction, for helical waveguides, we seek to identify transverse modes with a built-in cross sectional rotation, as defined next.

4.1. **Helical transverse modes.** Define a vector field $Z(x,y,z)$ on Ω by

$$Z = \big(T(\hat{z}) - \hat{x}\kappa T(\hat{z}) + \hat{x}\tau B(\hat{z}) - \hat{y}\tau N(\hat{z})\big) \circ \Phi^{-1}. \tag{4.1}$$

It has the property that $Z = T$ along the waveguide centerline. Moreover, its tangential components on any cross section $D(\hat{z})$ form a rotational vortex of strength determined by the torsion τ. We define a *propagating helical transverse mode* as any solution of the Helmholtz equation (2.14) of the form (2.17) satisfying an additional transversality condition that the directional derivative of U in the Z direction vanishes, i.e., propagating helical transverse modes are of the form

$$u(x,y,z) = e^{i\beta\, S(x,y,z)}\, U(x,y,z), \quad Z \cdot \nabla U = 0. \tag{4.2}$$

This is a strengthening of the prior ansatz (2.17). While the ansatz (2.17) posed no restriction at all on admissible solutions (since any solution can be brought to that form), now it is not even clear if there are Helmholtz solutions satisfying the revised ansatz (4.2). Later (in §5.5), we present ample numerical evidence pointing to the existence of such modes. Here we proceed to show why this is a very natural ansatz when viewed from the straightened configuration.

First note that coiled waveguides occurring in practice, ignoring any stress effects, when uncoiled, make a straightened waveguide whose material properties only vary along transverse cross sections (and not longitudinally along the propagation direction). To express this as a mathematical assumption, we use the previously defined straightened configuration and assume that $n(x,y,z)$ is such that $\hat{n} = n \circ \Phi$ has no longitudinal variations there, i.e.,

$$\hat{n}(\hat{x},\hat{y},\hat{z}) \equiv \hat{n}(\hat{x},\hat{y}) \quad \text{ is independent of } \hat{z}. \tag{4.3}$$

It is then natural to consider modes that also satisfy a similar assumption, i.e., to restrict the arbitrary 3D variation of $U(x,y,z)$ by assuming that $\hat{U} = U \circ \Phi$ is independent of $\hat{z}$ in the straightened configuration, i.e.,

$$\hat{U}(\hat{x},\hat{y},\hat{z}) \equiv \hat{U}(\hat{x},\hat{y}) \quad \text{ is independent of } \hat{z}. \tag{4.4}$$

Such an assumption is equivalent to restricting to propagating helical transverse modes defined in (4.2), as we now show.

Proposition 4.1. *Let Z be as in* (4.1). *The condition* (4.4) *holds for $\hat{U} = U \circ \Phi$ on $\hat{\Omega}$ if and only if*

$$Z \cdot \nabla U = 0 \qquad \text{in } \Omega. \tag{4.5}$$

Proof. Condition (4.4) is equivalent to $e_{\hat{z}} \cdot \hat{\nabla}\hat{U} = 0$, which, by (3.11), is the same as

$$(e_{\hat{z}} \cdot \hat{\nabla}\hat{U}) \circ \Phi^{-1} = e_{\hat{z}} \cdot \big([\nabla\Phi]^t \nabla U\big) = \big([\nabla\Phi] e_{\hat{z}}\big) \cdot \nabla U.$$

Since $[\nabla\Phi]e_{\hat{z}} = Z$ by (3.6), the result follows. □

4.2. **Two-dimensional model.** Let $\hat{D} = \hat{\Gamma}(0)$. It represents the (uniform) cross section of the straightened configuration $\hat{\Omega}$. Under the above assumptions, we are able to reduce the 3D eigenproblem to a 2D eigenproblem on $\hat{D}$. Define

$$r = \frac{1}{J^2}\begin{bmatrix} \tau\hat{y} \\ -\tau\hat{x} \end{bmatrix}, \qquad \mathcal{A} = \frac{1}{J^2}\begin{bmatrix} J^2+\tau^2\hat{y}^2 & -\tau^2\hat{x}\hat{y} \\ -\tau^2\hat{x}\hat{y} & J^2+\tau^2\hat{x}^2 \end{bmatrix}, \tag{4.6a}$$

with respect to the $e_{\hat{x}}, e_{\hat{y}}$ basis on $\hat{D}$. The matrix $\mathcal{A}$ can be alternately expressed as

$$\mathcal{A} = I_{2\times 2} + J^2 r r^t, \tag{4.6b}$$

where $I_{2\times 2}$ is the 2×2 identity matrix. Note that for a function $\hat{U}$ like in (4.4), the matrix $\mathcal{A}$ can be naturally applied to the gradient $\hat{\nabla}\hat{U} = e_{\hat{x}}\partial_{\hat{x}}\hat{U} + e_{\hat{y}}\partial_{\hat{y}}\hat{U}$ since it has no $\hat{z}$ component. We do not distinguish between the 2D and 3D vectors when the extra component vanishes. The 2D eigenproblem is to find a $\hat{U}$ satisfying (4.4) together with an eigenvalue β that solves

$$\begin{aligned} \hat{\mathrm{div}}(J\mathcal{A}\hat{\nabla}\hat{U}) + \hat{\imath}\beta\hat{\mathrm{div}}(Jr\hat{U}) + \hat{\imath}\beta Jr\cdot\hat{\nabla}\hat{U} + Jk^2\hat{n}^2\hat{U} = \beta^2 J^{-1}\hat{U}, &\quad \text{in } \hat{D}, \\ \hat{U} = 0, &\quad \text{on } \partial\hat{D}, \end{aligned} \tag{4.7}$$

where the divergence and the gradient are with respect to just the two variables $\hat{x}$ and $\hat{y}$. Its weak form (4.8) is displayed in the next result using $H_0^1(\hat{D})$, the Sobolev subspace of $L^2(\hat{D})$-functions on the 2D domain $\hat{D}$ whose derivatives are in $L^2(\hat{D})$ and whose trace vanishes on the boundary $\partial\hat{D}$. Any $\hat{U}$ in $H_0^1(\hat{D})$, being a function of $(\hat{x},\hat{y})$ in $\hat{D}$, is obviously independent of $\hat{z}$ and satisfies (4.4).

Theorem 4.2 (2D eigenproblem for helical transverse modes)**.** *Suppose* (4.3) *holds. Then any $\hat{U}$ in $H_0^1(\hat{D})$ and a real number β satisfies*

$$\begin{aligned} (J\mathcal{A}\hat{\nabla}\hat{U},\hat{\nabla}\hat{V})_{\hat{D}} - (Jk^2\hat{n}^2\hat{U},\hat{V})_{\hat{D}} + \beta\,\hat{\imath}\Big[(J\hat{U},r\cdot\hat{\nabla}\hat{V})_{\hat{D}} - (Jr\cdot\hat{\nabla}\hat{U},\hat{V})_{\hat{D}}\Big] \\ + \beta^2(J^{-1}\hat{U},\hat{V})_{\hat{D}} = 0 \end{aligned} \tag{4.8}$$

for all $\hat{V}\in H_0^1(\hat{D})$ if and only if β and $U = \hat{U}\circ\Phi^{-1}$ solves (2.20) *on the helical waveguide Ω.*

Proof. By Proposition 3.3, $U = \hat{U}\circ\Phi^{-1}$ solves (2.20) on Ω if and only if $\hat{U}$ solves (3.10) on $\hat{\Omega}$. We proceed to simplify the terms of (3.10) when (4.3) and (4.4) hold. For any W in $\mathcal{D}(\hat{\Omega})$,

$$\begin{aligned} \hat{a}(\hat{U},W) &= (J\mathcal{C}^{-1}\hat{\nabla}\hat{U},\hat{\nabla}W)_{\hat{\Omega}} - (Jk^2\hat{n}^2\hat{U},W)_{\hat{\Omega}} \\ &= \int_{-\infty}^{\infty}\int_{\hat{D}}\Big(J\mathcal{C}^{-1}\hat{\nabla}\hat{U}\cdot\hat{\nabla}\overline{W} - Jk^2\hat{n}^2\hat{U}\overline{W}\Big)\,d\hat{x}\,d\hat{y}\,d\hat{z} \\ &= \int_{\hat{D}}\left(J\mathcal{C}^{-1}\hat{\nabla}\hat{U}\cdot\left(\int_{-\infty}^{\infty}\hat{\nabla}\overline{W}\,d\hat{z}\right) - Jk^2\hat{n}^2\hat{U}\left(\int_{-\infty}^{\infty}\overline{W}\,d\hat{z}\right)\right)d\hat{x}\,d\hat{y} \\ &= \int_{\hat{D}}\Big(J\mathcal{C}^{-1}\hat{\nabla}\hat{U}\cdot\hat{\nabla}\overline{\hat{V}} - Jk^2\hat{n}^2\hat{U}\overline{\hat{V}}\Big)\,d\hat{x}\,d\hat{y}, \end{aligned}$$

where we have used in the penultimate step, the fact that J and $\mathcal{C}^{-1}$ are independent of $\hat{z}$ (as is clear from the expressions in Lemma 3.1, since the torsion and curvature of a helix are constant) as well as the $\hat{z}$-independence of $\hat{U}$ and $\hat{n}$ given by (4.3)–(4.4), and have put

$$\hat{V} = \int_{-\infty}^{\infty} W\,d\hat{z} \tag{4.9}$$

in the last step. Obviously, $\hat{V}$ is smooth, has no $\hat{z}$-dependence, and is in $\mathcal{D}(\hat{D})$. Moreover, since $\hat{W}$ has compact support, by the fundamental theorem of calculus, $\partial_{\hat{z}}\hat{V} = \int_{-\infty}^{\infty} \partial_{\hat{z}}\hat{W}\, d\hat{z} = 0$. Also noting that $\hat{\nabla}\hat{U}$ has no $e_{\hat{z}}$ component, we conclude that while computing the value of the integrand term $\mathcal{C}^{-1}\hat{\nabla}\hat{U} \cdot \hat{\nabla}\overline{\hat{V}}$, the last row and column of $\mathcal{C}^{-1}$ are multiplied by zero and are not seen. So we may replace $\mathcal{C}^{-1}$ with its 2×2 submatrix obtained by removing the last row and column of $\mathcal{C}^{-1}$, which is precisely the matrix $\mathcal{A}$. Thus we have proven that the first term of (3.10) simplifies to

$$\hat{a}(\hat{U}, W) = (J\mathcal{A}\hat{\nabla}\hat{U}, \hat{\nabla}\hat{V})_{\hat{D}} - (Jk^2\hat{n}^2\hat{U}, \hat{V})_{\hat{D}}.$$

Analogously, since r is the vector obtained from d by removing its last component, we prove that

$$\hat{b}(\hat{U}, W) = \hat{\imath}(J\hat{U}, r \cdot \hat{\nabla}\hat{V})_{\hat{D}} - \hat{\imath}(Jr \cdot \hat{\nabla}\hat{U}, \hat{V})_{\hat{D}},$$
$$\hat{c}(\hat{U}, W) = (J^{-1}\hat{U}, \hat{V})_{\hat{D}}.$$

Thus, given a $\hat{z}$-independent $\hat{U}$, if it satisfies (3.10) for all $W \in \mathcal{D}(\hat{\Omega})$, then (4.8) holds for all $\hat{V}$ of the form (4.9) and hence for all $\hat{V} \in \mathcal{D}(\hat{D})$. Since $\mathcal{D}(\hat{D})$ is dense in $H_0^1(\hat{D})$, one implication is proved. For the converse, if $\hat{U}$ in $H_0^1(\hat{D})$ solves (4.8), then retracing the above argument for $\hat{U}(\hat{x}, \hat{y})$ extended to $\hat{\Omega}$ constantly in $\hat{z}$, we find that (3.10) must hold for all 3D test functions $W \in \mathcal{D}(\hat{\Omega})$. Hence, the result is proved. □

4.3. **The toroidal limiting case.** In the limiting case when the angle α goes to zero, the helical waveguide becomes a ring, or a torus. Then (2.8) shows that $b_{\mathrm{H}} \to 0$ and both a_{H} and l approach the same value. (In this limit, as is clear from Figure 1, the helical centerline becomes a circle, so the waveguide becomes a torus.) In this limit, $\tau \to 0$ and $\kappa \to 1/a_{\mathrm{H}}$, as seen from (2.9). Hence, by (4.6), we have

$$\lim_{\alpha\to 0} J = 1 - \frac{\hat{x}}{a_{\mathrm{H}}}, \qquad \lim_{\alpha\to 0} r = \begin{bmatrix} 0 \\ 0 \end{bmatrix}, \qquad \lim_{\alpha\to 0} \mathcal{A} = I_{2\times 2}. \tag{4.10}$$

Then the 2D quadratic eigenproblem (4.8) reduces to the following *linear eigenproblem*

$$(J\hat{\nabla}\hat{U}, \hat{\nabla}\hat{V})_{\hat{D}} - (Jk^2\hat{n}^2\hat{U}, \hat{V})_{\hat{D}} = -\beta^2(J^{-1}\hat{U}, \hat{V})_{\hat{D}} \tag{4.11}$$

for the eigenvalue $-\beta^2$. Since there is no torsion in this torus limit case, there is no need for a cross-sectional rotation when considering mode transversality. Indeed, our general transversality condition $Z \cdot \nabla U = 0$ in (4.2), in the absence of torsion, simply reduces to the standard condition

$$T \cdot \nabla U = 0. \tag{4.12}$$

We caution however that (4.12) may not be appropriate for general helical waveguides.

Prior works on bent optical fiber waveguides—see [17] and its antecedents [9, 6]—have considered this toroidal case, where the fiber is deformed so that its inlet and outlet are fused to form a torus. For "slow bends," they proposed to account for the geometry of bending solely by replacing n with a modified effective index. In our notation (taking into account the direction of our N), their modified effective index equals the original index n scaled by a factor of $(1 - \hat{x}/a_{\mathrm{H}})$, which matches the above-found limiting value of J from our analysis. Nonetheless, as seen from (4.11), even for this simpler toroidal bending model, to be fully accurate, one must modify not only the term with n, but also the remaining two terms in the equation for modes.

4.4. **The upright limit.** The limiting case as α approaches $\pi/2$ is what we refer to as the upright limit. From (2.8), we see that this limit can be achieved either by fixing a_{H} to some positive number and letting b_{H} grow,

$$a_{\mathrm{H}} > 0, \qquad b_{\mathrm{H}} \to \infty, \qquad \alpha \to \frac{\pi}{2}, \tag{4.13}$$

or, by fixing b_{H} to some positive number and making a_{H} small,

$$b_{\mathrm{H}} > 0, \qquad a_{\mathrm{H}} \to 0, \qquad \alpha \to \frac{\pi}{2}. \tag{4.14}$$

In both cases, the helical waveguide approaches the shape of a straight upright cylinder centered around the z-axis. However, the two cases differ in their *limiting torsion:* in the case of (4.13), since $l \to \infty$, we see from (2.9) that the torsion τ approaches zero. In the case of (4.14), the torsion approaches $1/b_{\mathrm{H}}$. In both cases, the curvature κ approaches zero, and (4.6) gives

$$\lim_{\alpha\to\pi/2} J = 1, \qquad \lim_{\alpha\to\pi/2} r = \begin{bmatrix} \tau y \\ -\tau x \end{bmatrix}, \qquad \lim_{\alpha\to\pi/2} \mathcal{A} = I_{2\times 2} + r r^t.$$

where τ is understood to be the limiting torsion. The 2D quadratic eigenproblem (4.8), in this upright limiting case, reduces to

$$\begin{aligned} (\hat{\nabla}\hat{U}, \hat{\nabla}\hat{V})_{\hat{D}} + (r\cdot\hat{\nabla}\hat{U}, r\cdot\hat{\nabla}\hat{V})_{\hat{D}} - (k^2\hat{n}^2\hat{U}, \hat{V})_{\hat{D}} \\ + \beta\,\hat{\imath}\Big[(\hat{U}, r\cdot\hat{\nabla}\hat{V})_{\hat{D}} - (r\cdot\hat{\nabla}\hat{U}, \hat{V})_{\hat{D}}\Big] + \beta^2(\hat{U}, \hat{V})_{\hat{D}} = 0. \end{aligned} \tag{4.15}$$

In the case the upright limit is approached as in (4.13), since the limiting torsion τ vanishes, r becomes the zero vector, and (4.15) becomes a linear eigenproblem with $-\beta^2$ as the eigenvalue,

$$(\hat{\nabla}\hat{U}, \hat{\nabla}\hat{V})_{\hat{D}} - (k^2\hat{n}^2\hat{U}, \hat{V})_{\hat{D}} = -\beta^2(\hat{U}, \hat{V})_{\hat{D}}.$$

This is the familiar *linear eigenproblem for modes of an unbent straight waveguide* [16] with longitudinally constant material properties; and moreover, vanishing torsion also implies that the transversality condition reduces to the standard one (4.12).

However, if the upright limit is approached as in the other case (4.14), we must solve the quadratic eigenproblem. Note that we have *not* assumed that the material coefficient $n(x, y, z)$ is independent of z in the physical configuration Ω (even when Ω is a straight cylinder in the upright limit case). We have only assumed that (4.3) holds in the straightened configuration $\hat{\Omega}$. The map Φ, just (un)twists the straight cylinder Ω onto itself $\hat{\Omega} = \Omega$ in the situation of (4.14). Our setting allows inclusion of twisted material configurations contained within a straight cylinder, as in Figure 2, in this upright limit.

5. Numerical techniques and results

In this section, we use established numerical methods combined with a few new tricks to solve the previously formulated eigenproblems, and discuss the computational results, relating some to prior findings in the optics literature. In prior sections, we have introduced three eigenproblems for modes of a helical waveguide: *(i)* Proposition 2.2 gave a 3D eigenproblem on the physical helical waveguide, *(ii)* Proposition 3.3 gave a 3D eigenproblem on straightened configuration, and *(iii)* Theorem 4.2 gave a 2D eigenproblem on a waveguide cross section

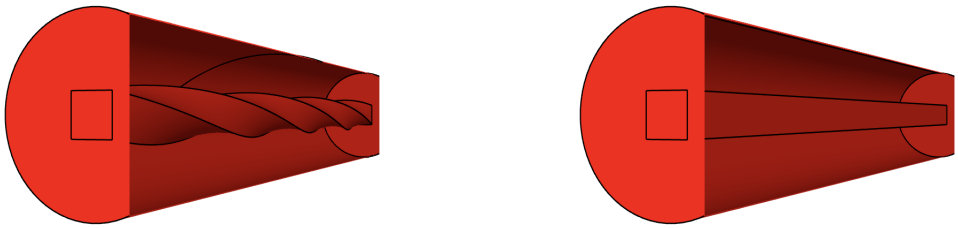

FIGURE 2. Assumption (4.3) allows for z-varying material configurations like the twisted rectangular core in the left figure (Ω) visible after clipping. The z-axis is into the page. The map Φ untwists it to the straightened configuration $\hat{\Omega}$ on the right.

after limiting the longitudinal variation of material coefficient by (4.3). In this section, we briefly describe how each of these eigenproblems can be numerical solved.

Of course, the 2D quadratic eigenvalue formulation (4.8) is the most attractive in practice since it is the least expensive and can be numerically solved with minimal tools. But we also compute with the 3D quadratic eigenvalue formulations in (3.10) and (2.20) for illustration and cross verification. The additional tools needed for the 3D eigenproblems are described in §5.2 (and the reader only interested in the 2D results may skip §5.2).

5.1. **Common tools for all three eigenproblems.** For all three eigenproblems, we discretize the underlying 2D or 3D spatial domain using a simplicial conforming finite element mesh $\mathcal{T}$, using curved elements as needed to fit the geometry accurately. Let $\mathcal{P}_\ell(\mathcal{T})$ denote the space of functions that are polynomials of degree at most ℓ in each mesh element. Each of the eigenproblems (2.20), (3.10), and (4.8), are discretized by replacing the infinite-dimensional Sobolev space there by its intersection with $\mathcal{P}_\ell(\mathcal{T})$, i.e., the Lagrange finite element subspace of order ℓ on the mesh. The default setting in our computations is $\ell = 4$. Using the Lagrange basis, one obtains in a standard way [7], a numerically solvable matrix version of the quadratic eigenproblem

$$(A_0 + \beta A_1 + \beta^2 A_2)x = 0, \tag{5.1}$$

where x is the vector of coefficients in the basis expansion of the wanted eigenfunction, and A_i are the finite element stiffness matrices of the three sesquilinear forms in the prior eigenproblem formulations. Since this process is completely standard, we omit further details.

To solve the sparse quadratic eigenproblem (5.1), we use the "FEAST algorithm" [4, 14], specifically its adaptation for polynomial eigenproblems in [5]. Finite element basis function calculations, matrix assembly, and visualization are performed using the open-source finite element library NGSolve [1, 18]. For reproducibility, the code for the benchmarks and computational results are publicly available in [11].

5.2. **Further computational techniques for the 3D formulations.** The 3D eigenvalue formulation in (2.20) was posed on an unbounded domain Ω. We need to rewrite it on a bounded domain before discretizing with finite elements. This can be done by exploiting the periodicity of the helix. A single period cell of the helical waveguide is obtained by starting from a cross section, say $D(0)$, and performing one complete round of the helix to arrive at $D(2\pi l)$. Note that the planes containing $D(0)$ and $D(2\pi l)$ are parallel (since $T(0) = T(2\pi l)$). The region of the waveguide Ω in between these parallel planes is the single period cell on which we compute, with periodic identification of corresponding points in $D(0)$ and $D(2\pi l)$.

To compute with (2.20), we also need the phase function S defined in (2.13) and its gradient, or at least approximations of them. Since S is not available analytically, this poses a problem. Our strategy to overcome it is to construct a finite element approximation to S using its values at some points. Since $\gamma \circ S$ equals the (orthogonal) closest point projection P, the value of $S(p)$ at any point $p \in \Omega$ must satisfy

$$(p - \gamma(S(p))) \cdot T(S(p)) = 0, \qquad p \in \Omega, \tag{5.2}$$

where γ and T are as in (2.1) and (2.7). On the tetrahedral mesh $\mathcal{T}$, we solve (5.2) on a collection of points $\{p_i\}$ with Newton's method. The points are selected to be the Gauss points used for numerical integration on the tetrahedra. To provide a good initial guess for the Newton iteration, we observe that in the simple case of a straight waveguide, $S(p) = z$, while in the other limit case of a torus, we have $S(p) = a_{\mathrm{H}}\,\theta(p)$, where $\theta(p)$ is the cylindrical angle of the point p measure from the x-axis in the xy-plane. Together they lead us to choose as initial guess $S_0(p) = z\,\sin\alpha + a_{\mathrm{H}}\,\theta(p)\,\cos\alpha$. Our numerical experience shows this to be a solid choice as long as $a_{\mathrm{H}} > R$, i.e., a "hole" is present when looking at the waveguide from above; otherwise, more sophisticated guesses or post-processing schemes might be needed.

Once $S_i := S(p_i)$ at the Gauss points have been (approximately) found by the Newton iterations, we construct the L^2 best approximation $S_h \in \mathcal{P}_\ell(\mathcal{T})$, with an ℓ that is consistent with the order of the selected Gauss points $\{p_i\}$, by

$$S_h = \operatorname*{arg\,min}_{\substack{R_h \in \mathcal{P}_\ell(\mathcal{T}) \\ R_h(x_i) = S_i}} \frac{1}{2}\|R_h\|^2_{L^2(\Omega)}. \tag{5.3}$$

Having the approximation S_h at hand, we can compute its element-wise gradient ∇S_h enabling us to solve the quadratic eigenproblem (2.18) approximately.

The next difficulty specific to the 3D case is that there are irrelevant (standing wave and non-propagating type) solutions of (2.20). We need a filtering mechanism to isolate the modes of interest from all computed modes. To isolate the propagating helical transverse modes, we use the definition (4.2) which uses the vector field Z in (4.1). However, computation of Z requires the inverse of Φ. It is not available analytically, but can be expressed using S. For any point p in Ω, $\hat{p} = \Phi^{-1}(p)$ in $\hat{\Omega}$ is given by

$$\Phi^{-1}(p) = \left((p - \gamma(S(p))) \cdot N(S(p)), (p - \gamma(S(p))) \cdot B(S(p)), S(p)\right).$$

Using the approximation S_h in place of S in this expression, we compute an approximation Z_h of Z and use $Z_h \cdot \nabla U = 0$ to isolate the relevant modes U.

We now turn to the 3D eigenproblem (3.10) on the straightened configuration. Here again, to get a computable version, we may consider one period cell, which in this case would be the bounded subset $\hat{\Omega}_1 = \hat{\Gamma}(0) \times [0, 2\pi l]$ of the unbounded domain $\hat{\Omega}$. However, now the periodicity is no longer relevant to the straightened geometry nor seen in the coefficients of (3.10). Hence, for efficiency, we compute on a smaller rescaled domain in $\hat{z}$ direction, $\hat{\Omega}_\sigma := \hat{\Gamma}(0) \times [0, 2\pi\, l/\sigma]$ with $\sigma > 1$. When *reducing* the height by a factor σ, the eigenvalues β of interest *scale* to $\sigma\beta$, since $\hat{c}(\hat{U}, \hat{V})$ scales by σ^{-2}, $\hat{b}(\hat{U}, \hat{V})$ scales by σ^{-1}, and $\hat{a}(\hat{U}, \hat{V})$ does not change for $\hat{U}$ and $\hat{V}$ that are constant in $\hat{z}$, a property that modes of interest possess. The identification of relevant modes is easy in this case: we only need to check that assumption (4.4) holds true, i.e., for a sequence of refined meshes we isolate modes $\hat{U}$ that satisfy $e_{\hat{z}} \cdot \hat{\nabla}\hat{U} = 0$.

5.3. **An optical fiber example.** Some of our numerical results are with parameters from a fiber optic waveguide. To facilitate description of such parameters, it is useful to note that a "step-index optical fiber" consists of a cylindrical core D_0 with cross section radius r_0 and a surrounding cladding $D_1 = D\backslash D_0$ of radius $r_1 > r_0$. Its refractive index n is modeled as a piece-wise constant function

$$n(x, y, z) = \begin{cases} n_0, & (x, y, z) \in D_0, \\ n_1, & (x, y, z) \in D_1, \end{cases} \tag{5.4}$$

where n_0 and n_1 are positive constants. Guided modes [2] of a (straight, unbent) step-index fiber can be analytically computed in terms of Bessel functions. They are localized around the core and exponentially decay away from the core within the cladding D_1. The cladding radius is usually an order of magnitude higher than the core radius, which permits the use of zero Dirichlet boundary conditions at the cladding's boundary. The operating signal wavelength determines the wavenumber k. Together these quantities define the nondimensional "V-number" (also called the "normalized frequency") [16] of the fiber,

$$V = r_0 k(n_0^2 - n_1^2). \tag{5.5}$$

The number of guided modes in the core depends [16, §5.2.1] on how large V is (and when V is smaller than the first root of the Bessel function J_0, there can only be one guided mode). The guided mode with the largest propagation constant β is called the fundamental mode.

In some numerical simulations (see §5.7) we use realistic values of r_i and n_i, but we begin reports of computational results in the next subsection by showing results from a simulation with unit-sized parameters. We shall use the above setting to compare the results from the 3D helical waveguide model (2.20), the 3D straightened configuration model (3.10), and the 2D model (4.8). Results from the 2D model are presented first.

5.4. **Numerical results from the 2D eigenproblem.** We use the setting from §5.3 but with (artificial) unit-sized parameters that correspond to a tightly wound thick helically coiled waveguide (see Figure 3), namely

$$r_0 = 1, \quad r_1 = 2.2, \quad a_{\mathrm{H}} = 3, \quad b_{\mathrm{H}} = 5/(2\pi), \quad V = 15, \quad n_1 = 1, \quad k = 1. \tag{5.6}$$

The value of n_0 is determined from (5.5). Thus, n is fixed from (5.4).

First, we report results obtained by solving the quadratic eigenproblem of the 2D model (4.8) with polynomial order $\ell = 4$ and a sequence of meshes where a representative mesh-size h is halved in each step. In the core, we used the mesh-size $h_c = h/2$. Five eigenmodes localized near the core that were found are displayed in Figure 3 and their corresponding propagation constants β_i are reported in Table 1. A clear convergence is observed in the table as the mesh size h is halved.

The corresponding eigenmodes are displayed (together with the 2D mesh) in the bottom row of Figure 3. All mode plots show the absolute value of the computed complex modes. The shift in localization from the core is clearly visible in these mode profiles. We have also mapped the 2D mode profiles onto a 3D waveguide schematic (top row of Figure 3) so the off-centered modal features can be placed correctly in the context of the physical waveguide's bend. Note that the Frenet normal, being the $\hat{x}$-axis in the 2D model, points to the origin

h	ne	ndof	β_1^2	β_2^2	β_3^2	β_4^2	β_5^2
1.6	72	605	13.735725166	7.554370381	6.381870597	1.213584120	0.599749013
0.8	91	763	13.735750272	7.554465932	6.381985947	1.213910004	0.599975761
0.4	349	2863	13.735759236	7.554485905	6.382002118	1.213986996	0.600030486
0.2	1509	12211	13.735759478	7.554486208	6.382002348	1.213987628	0.600030938
0.1	6108	49141	13.735759478	7.554486208	6.382002348	1.213987629	0.600030939
0.05	23842	191289	13.735759478	7.554486208	6.382002348	1.213987629	0.600030939

TABLE 1. Eigenvalues β^2 of the 2D model for a sequence of meshes with mesh-size h, number of triangular elements "ne", and number of degrees of freedom "ndof".

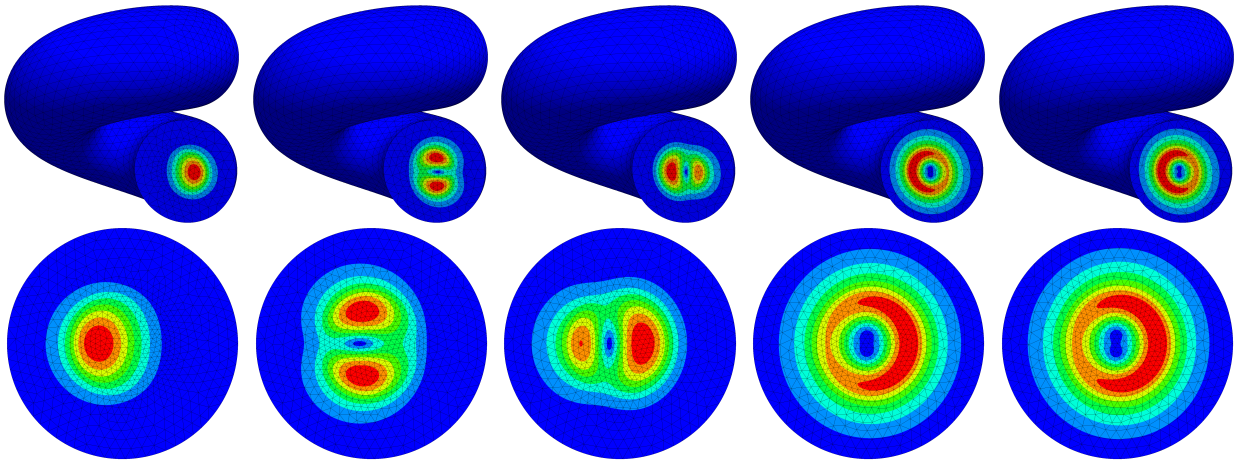

FIGURE 3. Magnitude of eigenmodes computed from the 2D model are illustrated in two ways: the bottom row shows them on the computed mesh; the top row shows them mapped onto the helically coiled waveguide. They are ordered left to right in descending order of their corresponding β-values in Table 1.

of the helix. Therefore, modes which shift to the left in the 2D setting, shift *outwards*, away from the coiling center, when placed in the 3D waveguide.

One reason for curving waveguides is to separate the fundamental mode from the higher-order modes. For a straight fiber with parameters (5.6), the eigenvalue of fundamental mode (LP01) can be analytically computed to be approximately 12.415638, whereas the next two higher order modes (LP11) are near 7.188311 (a difference of about 5.22) and the final two higher modes (LP21) are around 0.980593. From Table 1 we see that upon helical coiling, the fundamental mode's eigenvalue increased to 13.735759. Its closest higher-order mode is at 7.554486, making a separation of about 6.18. We see that the geometric effect of the helical coiling leads to better separation of the fundamental mode from the higher-order modes.

5.5. **Cross verification of results from the three eigenproblems.** Next, we proceed to cross verify the above results from the 2D model with 3D numerical results from the straightened configuration (3.10) and the physical helical waveguide (2.20). When computing with the straightened configuration we choose the scaling $\sigma = 4$ (see §5.2) to quarter the length of the cylinder in $\hat{z}$-direction (allowing for resources to be used to obtain better cross section resolution). We also compute the relative L^2-contribution of the $\hat{z}$-derivative of the

eigenmodes, via

$$\mathrm{err}_{\hat{z}} := \|\hat{\nabla}\hat{U} \cdot e_{\hat{z}}\|_{L^2(\hat{\Omega})} / \|\hat{\nabla}\hat{U}\|_{L^2(\hat{\Omega})} \tag{5.7}$$

to isolate modes of interest.

In Table 2 we show the results for the straightened configuration for three different meshes. We setup FEAST to search around the 2D eigenmodes with a search radius of 1 percent of the eigenvalue. In contrast to the 2D computations, we now obtain several eigenfunctions close to the desired eigenvalues. However, we found that (5.7) goes to zero only for five of them. The eigenvalues for those five modes converge to the 2D results in Table 1. This can be viewed as a numerical verification of our assumption (4.4) that there exists $\hat{z}$-independent eigenfunctions in the straightened configuration. The other computed modes, which have a high $\hat{z}$-derivative, are not propagating modes (but appear to be modes like standing waves). Their eigenvalues cluster around the relevant ones making it difficult to separate them looking only at the eigenvalues. However, (5.7) does effectively filter out the propagating modes of interest. The five modes are shown in Figure 4. We see the fundamental mode shifts along the Frenet normal, which is the $\hat{x}$-axis in the straightened configuration.

	ne=1376	ndof=15402	ne=9650	ndof=105604	ne=23309	ndof=253058
	β^2	$\mathrm{err}_{\hat{z}}$	β^2	$\mathrm{err}_{\hat{z}}$	β^2	$\mathrm{err}_{\hat{z}}$
β_1^2	13.733441557	0.076566	13.735758524	0.000252	13.735759215	0.000125
	13.763696206	0.866226	13.802052436	0.834760	13.522030691	0.957915
					13.802079895	0.834752
					13.664261602	0.993535
β_2^2	7.547275365	0.522232	7.554484798	0.000232	7.554485858	0.000112
	7.701110444	0.965881	7.505431057	0.904869	7.505437106	0.904868
	7.494815328	0.961366				
β_3^2	6.374972271	0.170528	6.382001254	0.000220	6.382002007	0.000110
			6.338427995	0.972767	6.261246381	0.991823
β_4^2	1.196704393	0.126262	1.213983256	0.000268	1.213986873	0.000130
	1.232101019	0.933150	1.202981316	0.383337	1.202986086	0.383336
β_5^2	0.594864213	0.389903	0.600027824	0.000271	0.600030404	0.000130
			0.607803431	0.383419	0.607806776	0.383419

TABLE 2. Eigenvalues β^2 of the 3D straightened configuration and their $\mathrm{err}_{\hat{z}}$ (defined in (5.7)) on a mesh with 1376 elements (15402 ndof, left), a mesh with 9650 elements (105604 ndof, middle), and a mesh with 23309 elements (253058 ndof, right).

As an additional cross verification, we compare the 2D results to the 3D modes computed using the original helical waveguide geometry (2.20). Again, three different meshes are used and the results from all three are in Table 3. To filter out propagating modes, we implement a numerical verification of (4.2) using the relative measure

$$\mathrm{err}_Z := \|\nabla U \cdot \tilde{Z}_h\|_{L^2(\Omega)} / \|\nabla U\|_{L^2(\Omega)}, \tag{5.8}$$

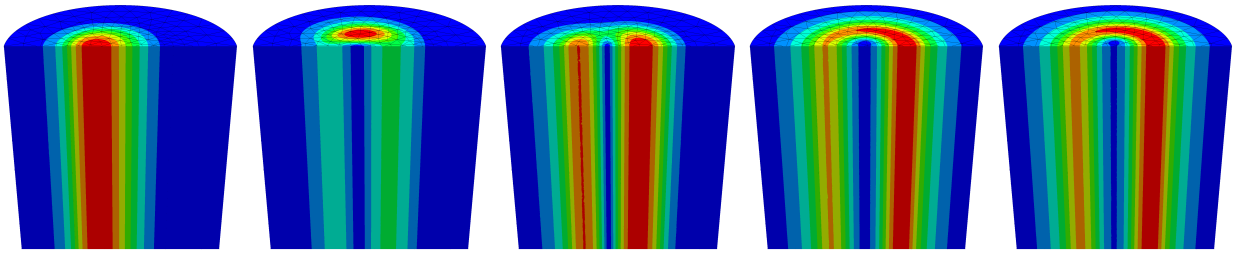

FIGURE 4. Visualization of selected modes and their off-center shift in the straightened configuration on the finest mesh. The $\hat{z}$-independence of these modes is apparent.

where $\tilde{Z}_h := Z_h/\|Z_h\|$ and Z_h is as described in §5.2. Filtering out the modes using (5.8) we again find five modes. As can be seen from Table 3, the eigenvalues computed on the bent waveguide do appear to converge to the 2D results of Table 1. The 3D results appear to be not as accurate because the mesh is comparably coarse. Also note that finer meshing of the waveguide appear to produce many more irrelevant eigenfunctions near the relevant ones, but we are able to use (5.8) to identify the propagating modes and only their eigenvalues appear to converge to the corresponding 2D eigenvalues. Needless to mention are the tremendous computational gains brought about by the 2D reduction (e.g., using a Mac M2 processor, the 2D computations for Table 1 took about 30 second, whereas the 3D computations in the straightened configuration to generate the results in Table 2 took about 1.25 hours).

5.6. **Comparing quadratic and linear eigenproblems for toroidal waveguide.** Consider the toroidal limit case $b_{\mathrm{H}} \to 0$ case described in §4.3. The limiting values of the geometric coefficients are described in (4.10). We numerically verify that in this case the 2D quadratic eigenproblem (4.8) is equivalent to the linear eigenproblem (4.11). We set the following parameter values

$$r_0 = 1, \quad r_1 = 2.2, \quad a_{\mathrm{H}} = 3, \quad b_{\mathrm{H}} = 0, \quad n_0 = 4, \quad n_1 = 1, \quad k = 1. \tag{5.9}$$

Note that this fiber has exactly the same V-number $V = 15$ as the previously considered case (5.6).

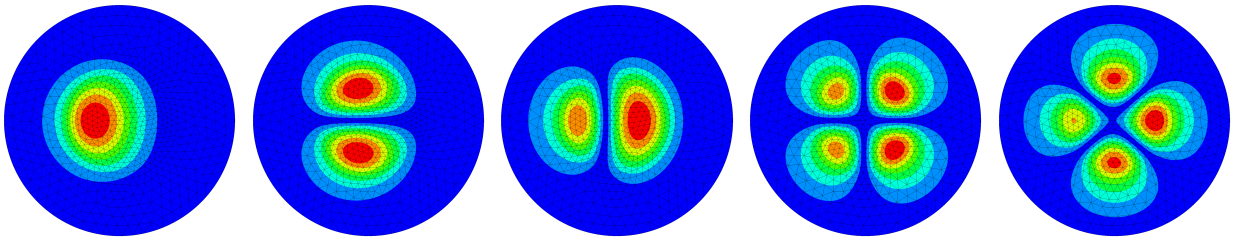

FIGURE 5. Magnitudes of the five eigenmodes on the cross section of the toroidal waveguide of (5.9). Results from the quadratic and linear eigenproblems are indistinguishable.

Figure 5 shows the modes computed from the 2D linear eigenproblem (4.11), where the limiting coefficient expressions for the torus from (4.10) are substituted. As the results from

	ne=4607 β^2	ndof=52318 err_Z	ne=7904 β^2	ndof=88372 err_Z	ne=17342 β^2	ndof=191630 err_Z
β_1^2	13.733206936	0.0953	13.734946168	0.0037	13.735732309	0.0011
	13.791778155	0.3427	13.480673401	0.7176	13.992433105	0.8126
	13.708566140	0.9150	13.518840973	0.6388	13.950479969	0.8705
			14.004442036	0.9569	13.499207778	0.7173
			13.860708691	0.9292	13.535777888	0.6385
			13.800827527	0.3403	13.677100791	0.9296
					13.753184231	0.9633
					13.802025335	0.3401
β_2^2	7.547335104	0.0237	7.553670129	0.0060	7.554449886	0.0008
	7.680087108	0.9041	7.688733573	0.8144	7.675878453	0.7443
	7.503380976	0.4295	7.570153365	0.9518	7.647479028	0.8140
			7.504762148	0.4299	7.450916889	0.9057
			7.500999833	0.9060	7.502148982	0.9528
					7.505415507	0.4289
β_3^2	6.374600241	0.0190	6.381326289	0.0031	6.381974976	0.0007
β_4^2	1.198328310	0.0244	1.212183510	0.0040	1.213903444	0.0009
			1.201164013	0.1087	1.202903051	0.1085
β_5^2	0.588948792	0.0252	0.598743993	0.0039	0.599970767	0.0009
	0.596613234	0.1115	0.606525591	0.1091	0.607748146	0.1090

TABLE 3. Eigenvalues β^2 of the 3D physical helical waveguide and their err_Z (defined in (5.8)) on a mesh with 4607 elements (52318 ndof, left), a mesh with 7904 elements (88372 ndof, middle), and a mesh with 17342 elements (191630 ndof, right).

h	ne	ndof	β_1^2	β_2^2	β_3^2	β_4^2	β_5^2
1.6	72	605	13.896655945	7.417666545	6.466435528	0.866180693	0.865656552
0.8	91	763	13.896678708	7.417750941	6.466551350	0.866426447	0.865937597
0.4	349	2863	13.896688049	7.417771578	6.466567837	0.866493270	0.865999900
0.2	1509	12211	13.896688301	7.417771898	6.466568067	0.866493808	0.866000431
0.1	6108	49141	13.896688301	7.417771898	6.466568067	0.866493809	0.866000431

TABLE 4. Eigenvalues β^2 corresponding to the modes in Figure 5 for the toroidal waveguide of (5.9).

the quadratic eigenvalue problem (4.8) coincide up to numerical rounding error precision, we do not show them. A convergence study can be found in Table 4. A comparison of the prior eigenvalues for the helical case in Table 1 show that the eigenvalues have indeed changed.

From the mode plots in Figure 5, we observe a squeezing of the mode profiles to the left (which translates to away from the center of the torus). Such shifts in core localization can also be seen in the prior work of [17] which also considered the toroidal bending case. It is interesting to compare the last two eigenmodes in the toroidal case (Figure 5) with their previous analogues in the helical case (in Figure 3). Remnants of the typical four-leaf pattern of the LP21 modes of the unbent fiber are still visible in the toroidal case in Figure 5, but are harder to discern in Figure 3 where they appear to have been partially fused together.

The corresponding eigenvalues in the last two columns of Table 4 are closer to each other than their two analogues in the last two columns of Table 1.

5.7. **Parameter study of eigenmodes for varying helix pitch.** In this subsection, we investigate how modes change with the pitch when an optical fiber is helically coiled. The influence of the bend radius on mode profiles has been studied in the toroidal case (where there is no pitch). Hence, we only report our investigations into the previously unknown case of variations with the pitch, holding the bend radius fixed. We now consider more realistic parameters, with all length units set to micrometers,

$$r_0 = 12.5, \quad r_1 = 20r_0, \quad n_1 = 1.52, \quad n_0 = \sqrt{0.1^2 + n_1^2}, \quad k = \frac{2\pi}{1.064},$$

(so the V-number is $V = 0.1kr_0$ and the wavelength is 1.064). The bend radius is fixed to $a_{\mathrm{H}} = 15500$.

b_{H}	β_1^2	β_2^2	β_3^2	β_4^2	β_5^2
1	80.929235	80.873286	80.851811	80.799593	80.796619
2500	80.927556	80.872003	80.851200	80.798888	80.796050
5000	80.923099	80.868627	80.849689	80.797098	80.794604
7500	80.917191	80.864234	80.847927	80.795010	80.792766
10000	80.911145	80.859847	80.846440	80.793213	80.791031
12500	80.905788	80.856069	80.845424	80.791893	80.789665
25000	80.892417	80.847261	80.844356	80.789422	80.787356
50000	80.888737	80.845129	80.844413	80.788620	80.787309
75000	80.888406	80.844917	80.844453	80.788391	80.787471
100000	80.888343	80.844845	80.844493	80.788276	80.787574
250000	80.888314	80.844733	80.844590	80.788065	80.787778
500000	80.888313	80.844697	80.844626	80.787994	80.787850
∞	80.888313	80.844661	80.844661	80.787922	80.787922

TABLE 5. Observed variations in eigenvalues β^2 as pitch b_{H} is varied are reported. The last row gives the analytical eigenvalues for straight fiber.

We start with a pitch of $b_{\mathrm{H}} = 1$. Then we increase the pitch keeping track of the fundamental mode and the next four higher-order modes. The results are shown in Figure 6 for $b_{\mathrm{H}} = 1, 5000, 10000, 12500, 25000, 50000, 75000, 100000$ and the corresponding eigenvalues in Table 5. Clearly, these increasing values of b_{H} lead to the upright limit case (4.13) of vanishing torsion. As discussed previously in §4.4, in this limit, we expect to obtain the eigenvalues of the unbent fiber. Indeed, the last few rows of Table 5 show that our numerical eigenvalues do appear to converge to those of the unbent fiber (included in the last row) as b_{H} continues to increase. We also observe from the absolute values of the eigenfunctions plotted in Figure 6 that they also appear to converge to modulus of corresponding modes for the straight fiber. The apparent radial symmetry of the modulus plots in the last row in Figure 6 may be jarring. While the fundamental mode (LP01) of a straight fiber is radially symmetric, the next higher order modes (LP11 and LP21) are not. In fact the real and imaginary parts (not displayed) of the second and third plots of the last row in Figure 6 do show the nonsymmetric two-leaf structure of LP11 modes, and those of fourth and fifth plots have

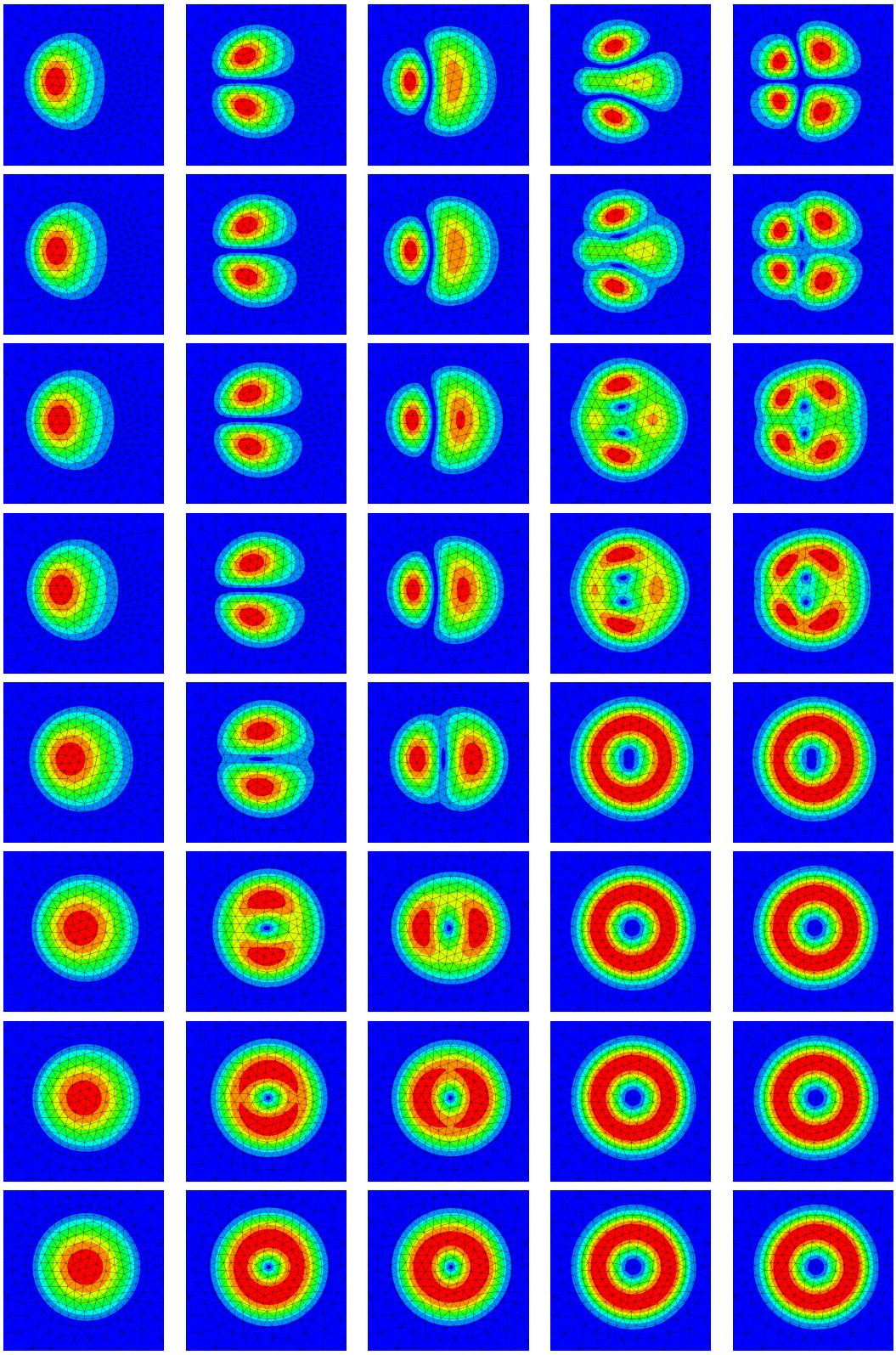

FIGURE 6. Changes in eigenmodes are visible as pitch is varied from the top row to the bottom row: $b_{\mathrm{H}} = 1, 5000, 10000, 12500, 25000, 50000, 75000, 100000$. Each column shows a different mode, with the first being the fundamental mode.

the four-leaf structure typical of LP21 modes. Their magnitudes however came out radially symmetric in our computations, as seen in the figure. Such modulus plots for modes close to LP11 and LP21 are perhaps atypical, but entirely possible. For double eigenvalues one may only expect convergence of eigenspaces (not individual eigenfunctions). We have indeed verified that the errors in the L^2 projections of the computed modes in Figure 6 onto the span of the corresponding LP modes of the straight fiber converge to zero as b_{H} increases.

Acknowledgments

This research was funded in part by the AFOSR grant FA9550-23-1-0103 and the Austrian Science Fund (FWF) under grant 10.55776/J4824. This work also benefited from activities organized under the auspices of NSF RTG grant DMS-2136228. For open access purpose, the authors have applied a CC BY public copyright license to any Author Accepted Manuscript (AAM) version arising from this submission.

References

[1] *NGSolve*. `https://ngsolve.org`.
[2] J. Bures, *Guided Optics*, Wiley, 2009.
[3] M. P. do Carmo, *Differential geometry of curves and surfaces*, Prentice-Hall, Inc., Englewood Cliffs, N.J., 1976.
[4] J. Gopalakrishnan, L. Grubišić, and J. Ovall, *Spectral discretization errors in filtered subspace iteration*, Mathematics of Computation, 89 (2020), pp. 203–228.
[5] J. Gopalakrishnan, B. Q. Parker, and P. Vandenberge, *Computing leaky modes of optical fibers using a FEAST algorithm for polynomial eigenproblems*, Wave Motion, 108 (2022), p. 102826.
[6] M. Heiblum and J. Harris, *Analysis of curved optical waveguides by conformal transformation*, IEEE Journal of Quantum Electronics, 11 (1975), pp. 75–83.
[7] F. Ihlenburg, *Finite element analysis of acoustic scattering*, vol. 132 of Applied Mathematical Sciences, Springer-Verlag, New York, 1998.
[8] D. Marcuse, *Curvature loss formula for optical fibers*, J. Opt. Soc. Am., 66 (1976), pp. 216–220.
[9] ——, *Influence of curvature on the losses of doubly clad fibers*, Applied Optics, 21 (1982), pp. 4208–4213.
[10] ——, *Light Transmission Optics*, van Nostrand Reinhold Company, 2 ed., 1982.
[11] M. Neunteufel and J. Gopalakrishnan, *Computational results and Python files for the work "Guided modes of helical waveguides"*, 2025.
[12] J. F. Nye, *Physical Properties of Crystals: Their Representation by Tensors and Matrices*, Oxford University Press, 1985.
[13] K. Olsen and J. Bohr, *The generic geometry of helices and their close-packed structures*, Theoretical Chemistry Accounts, 125 (2010), pp. 207–215.
[14] E. Polizzi, *A density matrix-based algorithm for solving eigenvalue problems*, Phys. Rev. B 79, 79 (2009), p. 115112.
[15] S. Przybył and P. Pierański, *Helical close packings of ideal ropes*, The European Physical Journal E, 4 (2001), pp. 445–449.
[16] G. A. Reider, *Photonics: An introduction*, Springer, Switzerland, 2016.
[17] R. T. Schermer and J. H. Cole, *Improved bend loss formula verified for optical fiber by simulation and experiment*, IEEE J. Quantum Elec., 43 (2007), pp. 899–909.
[18] J. Schöberl, *NETGEN an advancing front 2D/3D-mesh generator based on abstract rules*, Computing and Visualization in Science, 1 (1997), pp. 41–52.

Portland State University, PO Box 751, Portland OR 97201, USA
Email address: `gjay@pdx.edu`

Portland State University, PO Box 751, Portland OR 97201, USA
Email address: `mneunteu@pdx.edu`